Towards Gait-Pattern Adaptation Algorithms for Exoskeletons based on the ZMP Criterion

Marciel A. Gomes and Guilherme L. M. Silveira and Adriano A. G. Siqueira

Abstract— **This paper presents a gait-pattern adaptation algorithm for exoskeletons based on the Zero Moment Point criterion. The proposed exoskeleton is developed for lower limbs and based on a commercially available orthosis. The step length and duration are considered as the adaptation parameters, they are computed through minimization based on inverse dynamics and considering the orthosis-patient interaction forces. Also, a robust controller based on the $\mathscr{H}_\infty$ method is designed to attenuate the effects of external disturbances and parametric uncertainties in the trajectory tracking errors. The dynamic model of the actual exoskeleton, with interaction forces included, is used to generate simulation results.**

I. Introduction

The problem of gait-pattern adaptation for exoskeletons for lower limbs is considered in this paper. Robotic exoskeletons have being used to increase the physical capacity of soldiers in the military area [5], [14]. However, they also can be designed for helping physically weak or injured people during rehabilitation procedures [1].

Due to the importance of exercises for functional rehabilitation, the use of the robotics in this area is increasing [1]. The robotic orthosis Lokomat is being recently used for rehabilitation of patients with stroke or spinal cord injury individuals [3]. The device is installed in a treadmill and the patient walks using a weight compensator. A fixed gait-pattern is imposed through a joint position control of the robotic orthosis. To ensure the patient is not only having its leg moved passively for the locomotion device, gait-pattern adaptation algorithms are proposed in [4], [7], considering the human-machine interaction.

The proposed algorithms in [7] can not be applied directly for exoskeletons since they were developed for a fixed base robotic system, the Lokomat orthosis. They do not consider the stability of the gait-pattern. For exoskeleton, which can be considered as a biped robot, the generation of a stable walking pattern is an essential issue. In [2], it is presented a trajectory generator for biped robots taking into account the ZMP (Zero Moment Point) criteria [10]. Specific points of the ankle and hip trajectories are defined according to the desired step length and duration, and the minimization of a functional related to the ZMP. The cubic splines interpolation method is used to generate the complete trajectories. This method presents suitable results with smooth and second-order differentiable curves. The joint trajectories are obtained from the inverse kinematics. In [6], the trajectory generator proposed in [2] is extended for different ground inclinations and stairs.

In this paper it is proposed the combination of the stable trajectory generator described in [2] with the gait-pattern adaptation algorithms in [7] to generate stable trajectories for exoskeletons for lower limbs. The step length and duration are considered as the adaptation parameters, they are computed based on the inverse dynamic methodology proposed in [7]. The orthosis-patient interaction forces are considered in the dynamic model and used as input to the minimizing procedure. Simulation results are presented based on the dynamic parameters of an actual exoskeleton for lower limbs.

To ensure the orthosis-patient system follows the desired trajectory even in the presence of external disturbances and parametric uncertainties, a robust controller based on $\mathscr{H}_\infty$ performance is implemented. In [8], the authors present experimental results obtained from the implementation in robot manipulators of a nonlinear $\mathscr{H}_\infty$ control via quasi-linear parameter varying (quasi-LPV) representation . The quasi-LPV representation of a nonlinear system is a state-space equation where the system matrices are functions of state-dependent parameters [13]. In [9], a similar controller is proposed for disturbance attenuation considering a semi-passive dynamic walking of biped robots.

The papers is organized as follows: Section II presents the trajectory generator for biped robots with some issues related to the optimization procedure and ZMP stability criterion; Section III presents the dynamic model of the orthosis-patient system; Section IV deals with a robust controller design applied in the exoskeleton; Section V introduces the gait-pattern adaptation algorithm based on direct dynamics applied to exoskeletons; Section VI presents the results of the gait-pattern adaptation algorithms in the proposed exoskeleton model; and Section VII summarizes the main contributions of the paper.

II. Trajectory Generation with ZMP Criterion

In this section, the trajectory generator for biped robots presented in [2] is presented, with some considerations about the ZMP trajectory optimization. It is considered the exoskeleton as a biped robot with trunk, knees and feet, as shown in Figure 1. According to [2], the walking cycle can be divided in two phases, double support and single support. The double support phase starts when the heel of the forward foot touches the ground and finishes when the toe of the backward foot leaves the ground. The second phase is characterized by the fact only one foot is in contact with

The authors are with the Department of Mechanical Engineering, University of São Paulo at São Carlos, 400 Av. Trabalhador São-carlense - 13566-590, São Carlos-SP, Brazil siqueira@sc.usp.br

the ground. In this work, the double support represents 20% of the entire walking cycle.

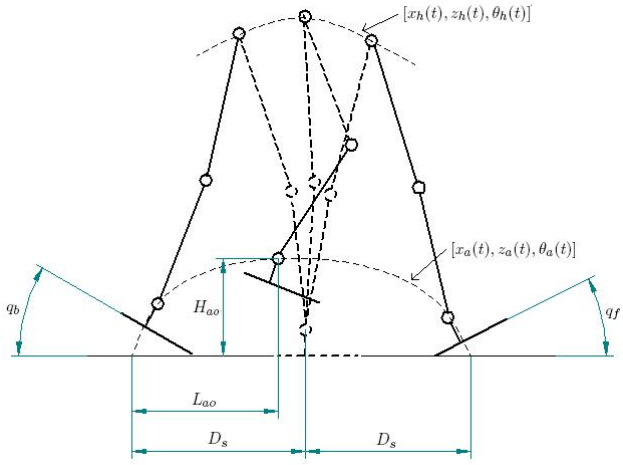

Fig. 1. Biped robot model.

Consider the inertia coordinate system of Figure 1. The foot and hip trajectories can be respectively parametrized as $X_a = [x_a(t), z_a(t), \theta_a(t)]^T$, where $(x_a(t), z_a(t))$ is the ankle position and $\theta_a(t)$ is the angle between the foot and the horizontal plane, and $X_h = [x_h(t), z_h(t), \theta_h(t)]^T$, where $(x_h(t), z_h(t))$ is the hip position and $\theta_h(t)$ is the angle between the trunk and the horizontal plane.

A. Foot Trajectory

The step k occurs between the kT_c and $(k+1)T_c$ time instants, where T_c is the step time interval. Step k is defined starting when the heel of any foot leaves the ground and finishing when the same heel touches the ground again, Figure 2. q_b and q_f are the angles of the foot with relation to the horizontal at the initial and final time instants of the swing phase (single support), respectively.

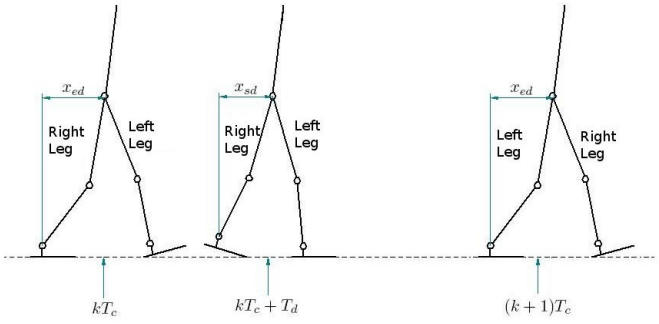

Fig. 2. Walking cycle, double and single support phases.

Assuming that the left foot is completely in contact with the ground during the times $kT_c + T_d$ and $(k+1)T_c$, the following conditions can be stated:

$$\theta_a = \begin{cases} q_{gs}(k), & t = kT_c \\ q_b, & t = kT_c + T_d \\ -q_f, & t = (k+1)T_c \\ -q_{ge}(k), & t = (k+1)T_c + T_d \end{cases} \quad (1)$$

where T_d is the time interval of the double support phase, $q_{gs}(k)$ and $q_{ge}(k)$ are the ground slope for the initial and final step instants, respectively.

The following specifications can also be defined for the foot position:

$$x_a = \begin{cases} kD_s, & t = kT_c \\ kD_s + l_{an} sin(q_b) & \\ \quad + l_{af}(1 - cos(q_b)), & t = kT_c + T_d \\ kD_s + L_{ao}, & t = kT_c + T_m \\ (k+2)D_s - l_{an} sin(q_f) & \\ \quad - l_{ab}(1 - cos(q_f)), & t = (k+1)T_c \\ (k+2)D_s, & t = (k+1)T_c + T_d \end{cases} \quad (2)$$

and

$$z_a = \begin{cases} h_{gs}(k) + l_{an}, & t = kT_c \\ h_{gs} + l_{af} sin(q_b) + l_{an} cos(q_b), & t = kT_c + T_d \\ H_{ao}, & t = kT_c + T_m \\ h_{ge} + l_{ab} sin(q_f) + l_{an} cos(q_f), & t = (k+1)T_c \\ h_{ge}(k) + l_{an}, & t = (k+1)T_c + T_d \end{cases} \quad (3)$$

where (L_{ao}, H_{ao}) is the higher foot position (this position occurs at $kT_c + T_m$), D_s is the step length, l_{an} is the foot height and l_{af} is the distance between the heel and the ankle joint. The heights of the ground when the foot is touching it are defined as $h_{gs}(k)$ and $h_{ge}(k)$, for the initial and final step instants, respectively. Some constraints on right foot velocities are also imposed, see [2] details.

A smooth trajectory can be generated through the interpolation method based on cubic splines, which generates a second order differentiable trajectory for all time interval.

B. Hip Trajectory

It is considered that the angle between the trunk and the horizontal axis $\theta_h(t)$ presents no variation along the walking cycle. Also, as the position of the ZMP is not affected by the hip motion in the z direction, it is assumed a little variation between the highest position H_{hmax} and the lowest position H_{hmin}, where the former occurs at the middle of the single support phase and the second at the middle of the double support phase. That is, z_h can be defined as:

$$z_h = \begin{cases} H_{hmin}, & t = kT_c + 0,5T_d \\ H_{hmax}, & t = kT_c + 0,5(T_c - T_d) \\ H_{hmin}, & t = (k+1)T_c + 0,5T_d. \end{cases} \quad (4)$$

Considering the sagittal plane, the hip motion along the x direction is the main contribution for the ZMP be inside the support polygon. In [2] it is proposed generate a set of stable trajectories $x_h(t)$ and select the trajectory with large stability margin according to the ZMP criterion.

The following conditions are defined for the hip trajectory along the x direction:

$$x_h = \begin{cases} kD_s + x_{ed}, & t = kT_c \\ (k+1)D_s - x_{sd}, & t = kT_c + T_d \\ (k+1)D_s + x_{ed}, & t = (k+1)T_c \end{cases} \quad (5)$$

where x_{sd} and x_{ed} are the distances along the x direction from the hip to the ankle of the support foot at the initial and final time instants of the swing phase, respectively. In this paper, these values are constrained to $x_{sd} \in (0; 0.5D_s)$ and $x_{ed} \in (0; 0.5D_s)$.

Considering the interpolation method based on cubic splines, it is possible to generate different trajectories and to select the best one according to the ZMP criterion. To ensure that the ZMP remains most of the time next to the center to the support polygon, the following functional is defined:

$$J(x_{ed}, x_{sd}) = \frac{\sum_{n=1}^{p} d_{ZMP}^2}{p}, \quad (6)$$

where d_{ZMP} is the distance between the ZMP and the center of the stability region defined by the convex polygon of the contact points and p is the number of points throughout the trajectory in which d_{ZMP} is computed.

C. Optimization Issues

The steepest descent algorithm was selected as the optimization method. It presents an easy implementation and high convergence rate after all parameters be adjusted. The computation of J is highly time consuming if a representative number of trajectory points p must be considered. The algorithm is defined as:

$$\overline{X}_{n+1} = \overline{X}_n - \eta \nabla J(x_{ed}, x_{sd}) \quad (7)$$

where $\overline{X}_n$ is the vector containing the values of x_{ed} and x_{sd} for optimization step n, η is the optimization rate and $\nabla J(x_{ed}, x_{sd})$ is the functional gradient with relation to x_{ed} and x_{sd}.

As shown in Section II-B, the minimization of J is constrained to $x_{sd} \in (0; 0.5D_s)$ and $x_{ed} \in (0; 0.5D_s)$. Hence, it is necessary to constrain the algorithm to these values. Also, there are values of x_{ed} and x_{sd} for which there is no solution for the inverse kinematic used to compute the shin and thigh absolute angles. The functional J is defined constant and equal to zero in this region.

If the result from optimization, $\overline{X}_{n+1}$, is outside the functional domain (where J is imposed to be zero), the optimization stops, because $\nabla J(x_{ed}, x_{sd}) = 0$. $\nabla J(x_{ed}, x_{sd})$ is computed numerically by a small variation on the parameters. According to the selected initial condition, the above problem occurs frequently if the optimization rate is not properly selected.

The following strategy was defined to solve this problem: if the optimization result belongs to the area outside the functional domain ($J = 0$ and $\nabla J = 0$), it is defined a convergence direction perpendicular to the last $\nabla J \neq 0$, until the result belongs to the domain. Figure 3 shows a minimization results where the proposed strategy is utilized and the final result is inside the functional domain.

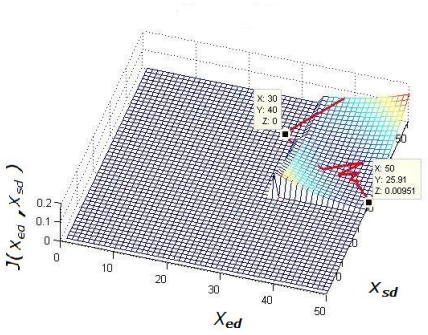

Fig. 3. Optimization results for initial value $\overline{X}_0 = [0.3\ 0.4]^T$ and optimal value $\overline{X}_{opt} = [0.5\ 0.26]^T$. The proposed strategy for points outside the functional domain is used at the second optimization step.

Figure 4 shows the surfaces of J for different values of D_s and T_c. This analysis is important because D_s and T_c define a essential characteristic of the gait-pattern, the velocity. By changing these parameters, a wide variation of trajectories can be created.

It can be noted from Figure 4 that the variation of T_c does not affect the surface of J. However, for a little variation on D_s the domain of J is extremely reduced. In this case, there is no solution for the inverse kinematic for a wide range of values. That is, there are few trajectories which maintain the hip height and develop a large step length, $D_s = 0.6$ m.

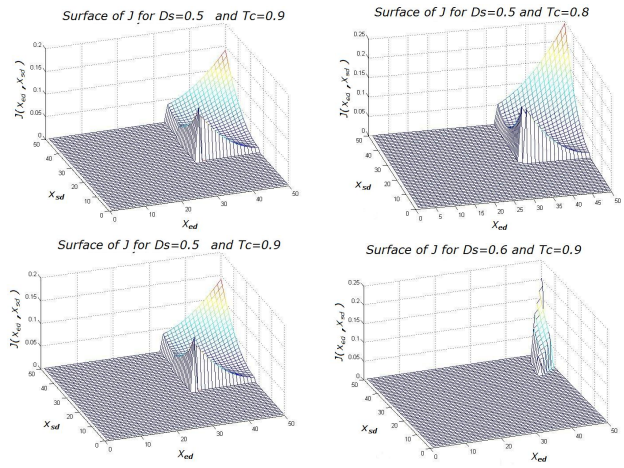

Fig. 4. Surfaces of J for different values of D_s and T_c.

From the analysis of the variation of J given a variation of D_s, it is proposed a relation between the step length, D_s, and the maximum height, H_{hmax}. For a given D_s, H_{hmax} can be computed as the height of the isosceles triangle defined by base D_s and sides $L_{th} + L_{sh}$ plus the ankle height. This value is parametrized by parameters defined as function of $(D_s - 0.5)$ an $(T_c - 0.9)$, the differences from the initial values of D_s and T_c, as shown in the following equations:

$$H_{hmax} = \left(\sqrt{(L_{sh} + L_{th})^2 - \left(\frac{D_s}{2}\right)^2} + l_{an} \right) . \alpha_1 . \alpha_2, \quad (8)$$

$$\begin{cases} \alpha_1 = \left(\frac{D_s-0.5}{0.5}\right)^2 - 1, & D_s - 0.5 > 0, \\ \alpha_1 = 1, & D_s - 0.5 < 0, \end{cases} \tag{9}$$

$$\alpha_2 = \left(\frac{|T_c - 0.9|}{0.9}\right)^{3.2} - 1. \tag{10}$$

where L_{sh} and L_{th} are the lengths of the shin and thigh, respectively.

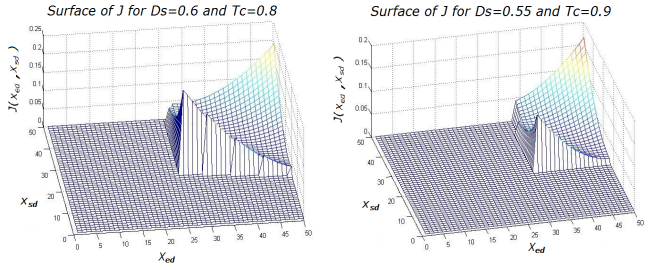

Fig. 5. Surfaces for J considering the empiric relation for H_{hmax}.

Figure 5 shows the surfaces for J computed for different values of D_s and considering the empirical relation for H_{hmax}. Note that the functional domain remains suitable for the optimization, even with the variation of D_s.

III. Quasi-LPV Representation of the Orthosis-Patient Dynamics

To implement the robust controller and the gait-pattern adaptation algorithm, the orthosis is modeled according to the basic robotic equation,

$$M_{ort}(q)\ddot{q} + C_{ort}(q,\dot{q}) + G_{ort}(q) = \tau_a + \tau_{pat} + \tau_d, \tag{11}$$

where $q \in \Re^n$ is the generalized coordinates vector, $M \in \Re^{nxn}$ is the symmetrical, positive definite inertia matrix, $C \in \Re^n$ is the centrifugal and Coriolis torques vector, and $G \in \Re^n$ is the gravitational torques vector. The terms $\tau \in \Re^n$ are the torques acting in orthosis: τ_a is the torque supplied by the actuators, τ_{pat} is the torque generated for the orthosis-patient interaction, and τ_d is the torque generated by any external disturbances acting in the patient-orthosis system.

The torque of interaction between the orthosis and the patient, τ_{pat}, can be divided in active and passive components. The passive patient torque, $\tau_{pat,pas}$, is the torque necessary to move the patient if he/she is moving in a passive way. In case that the patient influences in the orthosis movement, he/she will produce the active patient torque, $\tau_{pat,act}$. Therefore, Eq. (11) can be rewrite, considering now, the orthosis-patient dynamics,

$$\begin{aligned} M_{ort+pat}(q)\ddot{q} + C_{ort+pat}(q,\dot{q}) + G_{ort+pat}(q) \\ = \tau_a + \tau_{pat,act} + \tau_d, \end{aligned} \tag{12}$$

where $M_{ort+pat}(q)$, $C_{ort+pat}(q,\dot{q})$, and $G_{ort+pat}(q)$ correspond to the combination of the orthosis and patient dynamics.

The state tracking error is defined as:

$$\tilde{x} = \begin{bmatrix} \dot{q} - \dot{q}^d \\ q - q^d \end{bmatrix} = \begin{bmatrix} \dot{\tilde{q}} \\ \tilde{q} \end{bmatrix} \tag{13}$$

where q^d and $\dot{q}^d \in \Re^n$ are the desired reference trajectory and the corresponding velocity, respectively. The variables q^d, $\dot{q}^d$ and $\ddot{q}^d$, the desired acceleration, are assumed to be within the physical and kinematics limits of the exoskeleton.

The dynamic equation for the tracking error is given from (12) and (13) as

$$\dot{\tilde{x}} = A(q,\dot{q})\tilde{x} + Bu + Bw \tag{14}$$

with

$$\begin{aligned} A(q,\dot{q}) &= \begin{bmatrix} -M_{ort+pat}^{-1}(q)C_{ort+pat}(q,\dot{q}) & 0 \\ I_n & 0 \end{bmatrix} \\ B &= \begin{bmatrix} I_n \\ 0 \end{bmatrix} \\ w &= M_{ort+pat}^{-1}(q)\delta(q,\dot{q},\ddot{q}) \\ u &= M_{ort+pat}^{-1}(q)(\tau - M_{ort+pat}(q)\ddot{q}^d - C_{ort+pat}(q,\dot{q})\dot{q}^d \\ &\quad - G_{ort+pat}(q)), \end{aligned}$$

where $\delta(q,\dot{q},\ddot{q})$ are the composed disturbances defined as the sum of the external disturbances, τ_d, and the parametric uncertainties on the dynamic matrices $M_{ort+pat}(q)$, $C_{ort+pat}(q,\dot{q})$ and $G_{ort+pat}(q)$. The applied torque is given by:

$$\tau = M_{ort+pat}(q)(\ddot{q}^d + u) + C_{ort+pat}(q,\dot{q})\dot{q}^d + G_{ort+pat}(q).$$

Actually, the robust controller is working to attenuate only the effects of the external disturbances and the parametric uncertainties on the trajectory tracking errors. The active patient torque, $\tau_{pat,act}$, is not included into the composed disturbances, $\delta(q,\dot{q},\ddot{q})$, since it will be attenuated by the gait-pattern adaptation algorithm.

IV. State-feedback $\mathscr{H}_\infty$ Control

In this section it is presented the formulation and solution for the state-feedback $\mathscr{H}_\infty$ control problem for quasi-LPV systems, where the variyng parameters are function of the system states.

The tracking error dynamics shown in Eq. (14) is actually a quasi-LPV system, since, although the matrix $M_{ort+pat}(q)$ explicitly depends on the joint positions, we can consider it as function of the position error [8]:

$$M_{ort+pat}(q) = M_{ort+pat}(\tilde{q} + q^d) = M_{ort+pat}(\tilde{x},t).$$

The same can be observed for $C_0(q,\dot{q})$.

Consider the state-feedback control problem

$$\begin{aligned} \dot{x} &= A(\rho(x))x + B_1(\rho(x))w + B_2(\rho(x))u, \\ z_1 &= C_1(\rho(x))x, \\ z_2 &= C_2(\rho(x))x + u \end{aligned} \tag{15}$$

where $x \in \Re^n$ is the state, $u \in \Re^{q_2}$ is the control input, $w \in \Re^p$ is the disturbance input, $z_1 \in \Re^{q_1}$ and $z_2 \in \Re^{q_2}$ are system

outputs, $A(\cdot)$, $B_1(\cdot)$, $B_2(\cdot)$, $C_1(\cdot)$ and $C_2(\cdot)$ are continuous matrices of proper dimensions and $\rho(x) \in F_P^{\nu}$, defined by

$$F_P^{\nu} = \left\{\rho \in \mathscr{C}^1(\Re^+, \Re^m) : \rho(x) \in P, |\dot{\rho}_i| \leq \nu_i, i = 1, \ldots, m\right\},$$

where $P \subset \Re^m$ is a compact set, and $\nu = [\nu_1 \cdots \nu_m]^T$ with $\nu_i \geq 0$. The system (15) presents $\mathscr{L}_2$ *gain* $\leq \gamma$ in the interval $[0, T]$ if

$$\int_0^T \|z(t)\|_2^2 dt \leq \gamma^2 \int_0^T \|w(t)\|_2^2 dt, \tag{16}$$

for all $T \geq 0$, all $w \in \mathscr{L}_2(0, T)$ with the system starting from $x(0) = 0$ and $z(t) = [z_1(t)^T \;\; z_2(t)^T]^T$. The objective is to find a continuous function $F(\rho(x))$, such that the system in closed-loop presents $\mathscr{L}_2$ *gain* $\leq \gamma$ with state-feedback law $u = F(\rho(x))x$. This problem was solved in [13] and the solution is given in the following.

If there exists a continuous differentiable function $X(\rho(x)) > 0$ for all $\rho(x) \in P$ that satisfies

$$\begin{bmatrix} G(\rho) & X(\rho)C_1^T(\rho) & B_1(\rho) \\ C_1(\rho)X(\rho) & -I & 0 \\ B_1^T(\rho) & 0 & -\gamma^2 I \end{bmatrix} < 0, \tag{17}$$

where

$$G(\rho) = -\sum_{i=1}^{m} \pm\left(\nu_i \frac{\partial X}{\partial \rho_i}\right) + \widehat{A}(\rho)X(\rho) + X(\rho)\widehat{A}^T(\rho) - B_2(\rho)B_2^T(\rho)$$

and $\widehat{A}(\rho) = A(\rho) - B_2(\rho)C_2(\rho)$, then, with state-feedback law

$$u = -(B_2^T(\rho)X^{-1}(\rho) + C_2(\rho))x, \tag{18}$$

the closed-loop system has $\mathscr{L}_2$ *gain* $\leq \gamma$ for all parameter trajectories $\rho(x) \in F_P^{\nu}$.

Note that (17) actually represents 2^m inequalities and $\sum \pm(\cdot)$ indicates that every combination $+(\cdot)$ and $-(\cdot)$ should be satisfied. A practical scheme ([13], [8]) can be used to solve the infinite dimensional convex optimization problem represented by (17). First, choose a set of $\mathscr{C}^1$ functions, $\{f_i(\rho(x))\}_{i=1}^M$, as base for $X(\rho)$, i.e.,

$$X(\rho(x)) = \sum_{i=1}^{M} f_i(\rho(x))X_i,$$

where $X_i \in S^{n \times n}$ is the matrix coefficient for $f_i(\rho(x))$.

Second, the parameters set P is divided in L points, $\{\rho_k\}_{k=1}^L$, in each dimension. Since (17) consists in 2^m entries, a total of $(2^m + 1)L^m$ matrix inequalities in term of matrices $\{X_i\}$ should be solved.

V. Gait-Pattern Adaptation Algorithm

In this section an adaptation algorithm based on direct dynamics is used to generated the trajectory parameters D_s and T_c according to the interaction between the orthosis and the user. Consider the acceleration of the generalized coordinates,

$$\ddot{q} = M_{ort+pat}^{-1}(q)\left\{\tau_a + \tau_d - C_{ort+pat}(q, \dot{q}) - G_{ort+pat}(q)\right\} + M_{ort+pat}^{-1}(q)\,\tau_{pat,act}. \tag{19}$$

Inspecting Eq. (19), it can be observed that the last term represents the variation in the acceleration of the reference trajectory imposed for the patient. This hypothesis forms the base of the adaptation algorithm based on direct dynamics. The idea is to estimate the term $\tau_{pat,act}$ via force measurement and calculate the variation in acceleration. Adding the measured variation to the nominal acceleration, it is defined the patient desired acceleration,

$$\delta\ddot{q} = -M_{ort+pat}^{-1}(q)\,\delta\tau_{pat,act} \Rightarrow \ddot{q}_{des,pat} = \ddot{q}_{nom} + \omega\delta\ddot{q}, \tag{20}$$

where w is an adaptation constant. The adaptation of parameters D_s and T_c is carried through via minimization of the following functional,

$$J(\delta q_r, F) = \sum \left\|\ddot{q}_{des,pat}(\tau_{pat,act}) - \ddot{q}_{adap}(\delta q_r)\right\|_2^2. \tag{21}$$

Again the steepest descent method describe in Section II-C is used to minimize the functional $J(\delta q_r, F)$. An important advantage of the direct dynamics is the less dependence of the model; only the knowledge of inertia matrix $M_{ort+pat}(q)$ is necessary.

VI. Simulation Results

The orthosis used for the exoskeleton for lower limbs corresponds to one Reciprocating Gait Orthosis LSU (Lousiana State University). Figure 6 shows the orthosis and the exoskeleton design, created in the Solid Egde software. It is considered that all joint in the sagittal plane will be driven by an Series Elastic Actuator (SEA). SEA can performed force and impedance controls, which can be used to generate a variable impedance controller [11].

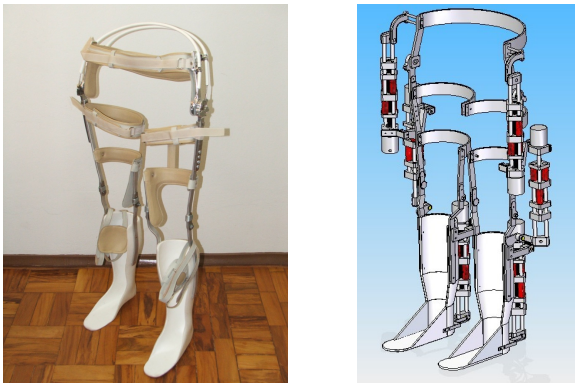

Fig. 6. RGO orthosis and exoskeleton design (Solid Edge).

The dynamic parameters of the orthosis, shown in Tab. I, was obtained by the Solid Edge model. It is also presented the parameters of the patient considered in the simulation, obtained from [12], considering a 85 kg, 1.74 m individual.

An analytical model of the orthosis, considering the patient interaction and ground reaction forces, is developed using the Symbolic Toolbox of the Matlab. Figure 7 shows the motion animation of the orthosis-patient system for a simulation of two steps. In the initial step it is considered $D_s = 0.45$ and $T_c = 0.9$. For the second step $D_s = 0.58$ and $T_c = 0.8$. Only the orthosis representation is shown since the patient dynamic is incorporated in the orthosis dynamics.

TABLE I

ORTHOSIS AND PATIENT DYNAMIC PARAMETERS.

Orthosis		**Patient**	
$M_{total,ort}$	4.8	$M_{total,pat}$	85
$L_{total,ort}$	1.0	$L_{total,pat}$	1.74
Limb Mass (kg)			
$M_{tigh,ort}$ 0.95		$M_{tigh,pat}$	8.5
$M_{leg+foot,ort}$	0.72	$M_{leg+foot,pat}$	5.2
$M_{torso,ort}$	1.49	$M_{torso,pat}$	57.6
Limb Length (m) - z direction			
$L_{tigh,ort}$	0.39	$L_{tigh,pat}$	0.39
$L_{leg+foot,ort}$	0.49	$L_{leg+foot,pat}$	0.49
$L_{torso,ort}$	0.12	$L_{torso,pat}$	0.87

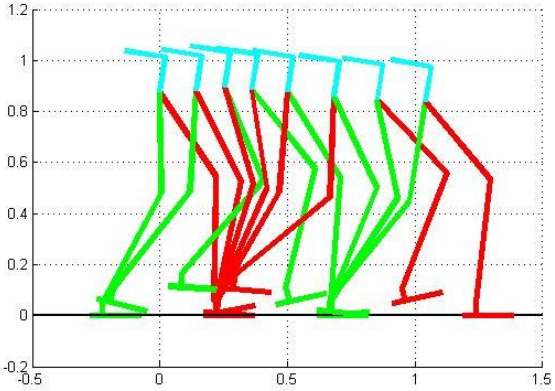

Fig. 7. Motion animation of the orthosis-patient system.

In this section, the gait-pattern adaptation algorithm presented in Section V is implemented in the model of the orthosis of Fig. 6. The initial desired trajectory, considered here as the nominal one, is defined by $D_s = 0.5$ and $T_c = 0.9$.

Because only simulation is performed in this work, the interaction torque between orthosis and patient (active patient torque) must be artificially estimated from a definite trajectory. In this work, this value is computed through the comparison between the desired trajectory for the patient, q^d_{pat} and the actual desired trajectory, q^d. It is assumed that the interaction torque results of a spring type virtual coupling between the patient desired position and the real position,

$$\tau_{pat,act} = K\left(q^d_{pat} - q^d\right). \tag{22}$$

The spring stiffness is adjusted in order to take realistic magnitudes of the active patient torque. For sake of simplicity, the desired trajectory of the patient is defined by $D_s = 0.54$ and $T_c = 0.86$. These parameters represent an increase of approximately 13% in the walking velocity. The adaptation of the parameters D_s and T_c is conducted at the end of the step (off-line, this procedure is possible in this type of adaptation), considering five equally spaced points throughout the step time.

The values of the parameters are then updated as nominal trajectory and a new step of the orthosis-patient model simulation is performed. The value of ω used in the algorithm based on the direct dynamics is 0.5. The final adapted parameters after two sequences of optimizations of the parameters, are $D_s = 0.5425$ and $T_c = 0.8572$. Figure 8 presents the nominal, patient desired, adapted and actual trajectories of the left shin, referring three steps, initiating with the right leg in stance. Note that at the second step, after $t = 1$ s, the adapted trajectory comes close to the patient desired trajectory.

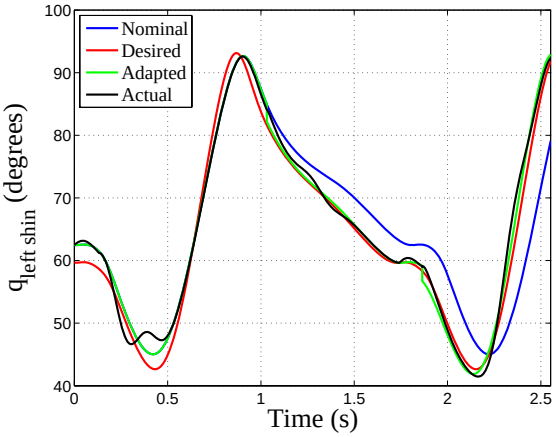

Fig. 8. Nominal, patient desired, adapted and actual trajectories of the left shin, absolute angle.

It can be observed that the algorithm obtained satisfactory results with relation to the adaptation of the parameters used in the patient desired trajectory. Also, note that the algorithm has good results just at the beginning of the second walking cycle. Thus, the necessary time for the adaptation of the trajectory is small, showing the functionality of the algorithm.

External disturbances acting in the patient-orthosis joints can be simulated as additional torques applied to the actuators. In this paper, it is considered in the simulation external disturbances composed of normal and sine functions, see [9] for details. From Figure 8 it can be verified that the robust controller rejected the external disturbances applied at the initial part of each step.

VII. CONCLUSIONS

This paper presents the first results of the development of an exoskeleton for lower limbs based on a reciprocating gait orthosis. It is presented the implementation of a gait-pattern adaptation algorithm which considers orthosis-patient interaction forces and the ZMP criterion, allowing the patient to modify the gait-pattern as his/her degree of voluntary locomotion still maintaining the walking stability. A robust controller is proposed to attenuate the deviations from the desired trajectories due to external disturbances and parametric uncertainties. The simulation results show the proposed adaptation algorithms can be applied in the actual exoskeleton being constructed.

REFERENCES

[1] D. P. Ferris, G. S. Sawicki, and A. R. Domingo. Powered lower limb orthoses for gait rehabilitation. *Top Signal Cord inj. Rehabilitation*, 11(2):34–49, 2005.

[2] Q. Huang, K. Yokoi, S. Kajita, K. Kaneko, H. Arai, N. Koyachi, and K. Tanie. Planning walking patterns for a biped robot. *IEEE Transactions on Robotics and Automation*, 17(3), 2001.

[3] S. Jezernik, G. Colombo, T. Keller, H. Frueh, and M. Morari. Robotic orthosis Lokomat: A rehabilitation and research tool. *Neuromodulation*, 6(2):108–115, 2003.

[4] S. Jezernik, G. Colombo, and M. Morari. Automatic gait-pattern adaptation algorithms for rehabilitation with a 4-dof robotic orthosis. *IEEE Transactions on Robotics and Automation*, 20(3):574–582, 2004.

[5] H. Kazerooni. Exoskeletons for human power augmentation. In *Proceedings of the 2005 IEEE/RSJ International Conference on Intelligent Robots and Systems*, Edmonton,Canada, 2005.

[6] P. N. Mousavi, C. Nataraj, A. Bagheri, and M. Alizadeh Entezari. Mathematical simulation of combined trajetory paths of a seven link biped robot. *Applied Mathematical Modelling*, 32:1445–1462, 2008.

[7] R. Riener, L. Lnenburger, S. Jezernik, M. Anderschitz, G. Colombo, and V. Dietz. Patient-cooperative strategies for robot-aided treadmill training: First experimental results. *IEEE Transactions on Neural Systems and Rehabilitation Engineering*, 13(2):380–394, 2005.

[8] A. A. G. Siqueira and M. H. Terra. Nonlinear and markovian $\mathscr{H}_\infty$ controls of underactuated manipulators. *IEEE Transactions on Control Systems Technology*, 12(6):811–826, 2004.

[9] A. A. G. Siqueira and M. H. Terra. Nonlinear $\mathscr{H}_\infty$ control applied to biped robots. In *Proceedings of the 2006 IEEE Conference on Control Applications (CCA06)*, Munich, Germany, 2006.

[10] M. Vukobratovic and D. Juricic. Contribution to the synthesis of biped gait. *IEEE Trans. Bio-Medical Engineering*, BM-16(1), 1969.

[11] C. J. Walsh, D. J. Paluska, K. Pasch, W. Grand, A. Valiente, and H. Herr. Development of a lightweight, underactuated exoskeleton for load-carrying augmentation. In *Proceedings of the 2006 IEEE International Conference on Robotics and Automation*, Orlanda, Florida, 2006.

[12] D. A. Winter. *Biomechanics and motor control of human gait*. John Wiley Interscience, 2 edition, 1990.

[13] F. Wu, X. H. Yang, A. Packard, and G. Becker. Induced $\mathscr{L}_2$-norm control for LPV systems with bounded parameter variation rates. *International Journal of Robust and Nonlinear Control*, 6(9/10):983–998, 1996.

[14] A. Zoss, A. Chu, and H. Kazerooni. Biomechanical design of the Berkeley Lower Extremity Exoskeleton (BLEEX). *IEEE/ASME Transactions on Mechatronics*, 11(2):128–138, 2006.